Title	GHz bandwidth semipolar (112¯2) InGaN/GaN light-emitting diodes
Author(s)	Dinh, Duc V.; Quan, Zhiheng; Roycroft, Brendan; Parbrook, Peter J.; Corbett, Brian
Publication date	2016-12-12
Original citation	Dinh, D. V., Quan, Z., Roycroft, B., Parbrook, P. J. and Corbett, B. (2016) 'GHz bandwidth semipolar (112¯2) InGaN/GaN light-emitting diodes', Optics Letters, 41(24), pp. 5752-5755. doi: 10.1364/OL.41.005752
Type of publication	Article (peer-reviewed)
Link to publisher's version	http://dx.doi.org/10.1364/OL.41.005752 Access to the full text of the published version may require a subscription.
Rights	**© 2016, Optical Society of America. One print or electronic copy may be made for personal use only. Systematic reproduction and distribution, duplication of any material in this paper for a fee or for commercial purposes, or modifications of the content of this paper are prohibited.**
Item downloaded from	http://hdl.handle.net/10468/11143

GHz bandwidth semipolar $(11\bar{2}2)$ InGaN/GaN light-emitting diodes

DUC V. DINH[1,*], ZHIHENG QUAN[1,2], BRENDAN ROYCROFT[1], PETER J. PARBROOK[1,2], AND BRIAN CORBETT[1]

[1] *Tyndall National Institute, University College Cork, Lee Maltings, Dyke Parade, Cork, Ireland*
[2] *School of Engineering, University College Cork, Cork, Ireland*
[*] *Corresponding author: duc.vn.dinh@gmail.com*

Compiled November 8, 2016

We report on the electrical-to-optical modulation bandwidths of non-mesa-etched semipolar $(11\bar{2}2)$ InGaN/GaN light-emitting diodes (LEDs) operating at 430 - 450 nm grown on high quality $(11\bar{2}2)$ GaN templates, which were prepared on patterned *r*-plane $(10\bar{1}2)$ sapphire substrates. The measured frequency response at -3 dB of the LEDs was up to 1 GHz. A high back-to-back data transmission rate of above 2.4 Gbps is demonstrated using a non-return-to-zero on-off keying modulation scheme. This indicates that $(11\bar{2}2)$ LEDs are suitable Gbps data transmission for use in visible-light communication applications.

OCIS codes: (060.2605) Free-space optical communication; (060.2630) Frequency modulation; (230.2090) Electro-optical devices; (230.3670) Light-emitting diodes

http://dx.doi.org/10.1364/ao.XX.XXXXXX

Visible-light communications (VLC) have significantly increased in popularity with the development of solid-state lighting. This is due to the major achievements in InGaN quantum-well (QW) active region based visible light-emitting diodes (LEDs) [1]. With the strong increase of wireless (Wi-Fi) applications which makes more considerable use of the limited radio-frequency (RF) spectrum, tapping into the optical portion of the spectrum alleviates the issue of "spectral deficiency" [2]. VLC provides a harmless technique to both private and public communications including indoor home communications, underwater communications, optical Wi-Fi for local-area-network (LAN) applications, vehicular communications, and machine to machine communications [2]. Additionally, VLC has no electromagnetic interference (EMI) to the existing Wi-Fi devices. Thus, VLC has a significant potential to supplement the existing RF-based Wi-Fi communications.

The frequency response at -3 dB ($f_{\text{-3 dB}}$) of conventional LEDs (phosphor-based LEDs and single-colour LEDs) is limited by the carrier radiative lifetime (τ_R) and the parasitic capacitance [2]. The lifetime decreases with increasing carrier density and by stimulated emission. Additionally, for InGaN-based LEDs, the spatial overlap of the electron and hole wave-functions in the QW active region plays a role as the built-in field in (0001) polar structures separates the carriers and thereby increases the radiative lifetime [3]. These devices can also be limited by the phosphor lifetime (1-mm^2-sized chips) [2]. Together with the output resistance of the driver circuit, $f_{\text{-3 dB}}$ of these devices is limited to a few tens of MHz [2, 4, 5]. There has been an effort made to increase this rate of (0001) LEDs by mesa-etching (shaping) LEDs to μm size [6–11]. Additionally, the parasitic capacitance of μ-LEDs has been found to reduce [10, 12], and hence $f_{\text{-3 dB}}$ can be further increased [7, 10]. Recently, the highest $f_{\text{-3 dB}}$ of 833 MHz has been realized for 24-μm-diameter (0001) LEDs at an injection current density (J_{inject}) of $\sim$16 kA/cm^2 [11]. For (0001) LEDs, the efficiency droop becomes more significant at higher J_{inject} [13, 14]. This droop has been found to affect the performance and an increased error rate of data transmission rate in (0001) LED-based VLC systems [15].

For InGaN QWs grown along semipolar oriented surfaces, the polarization-related electric fields have theoretically been predicted to significantly reduce that should lead to a reduced τ_R [3]. This has been experimentally confirmed in $(20\bar{2}1)$ [16] and $(11\bar{2}2)$ InGaN QWs [17] by time-resolved photoluminescence. Additionally, due to these reduced fields, the efficiency droop in semipolar LEDs in comparison with polar LEDs has been found to be much smaller [18, 19]. It is therefore expected that semipolar LEDs should be a good candidate for high-speed VLC systems. However, there are a very few studies that have been dedicated to investigate this potential application in blue and green $(11\bar{2}2)$ LEDs operating at 450 nm [20, 21] and 500 nm [20], a violet $(20\bar{2}\bar{1})$ superluminescent diode (SLD) operating at 405 nm [22], a blue $(20\bar{2}\bar{1})$ SLD operating at 447 nm [23], and a violet $(20\bar{2}\bar{1})$ laser diode (LD) operating at 410 nm [24]. For $(11\bar{2}2)$ LEDs [20], $(20\bar{2}\bar{1})$ SLD [22], and $(20\bar{2}\bar{1})$ LD [24], $f_{\text{-3 dB}}$ values of 480 MHz (J_{inject} = 110 A/cm^2), 807 MHz (J_{inject} = 17 kA/cm^2), and 5 GHz (J_{inject} = 9.2 kA/cm^2) have been reported, respectively.

In this Letter, we investigated the electrical-to-optical $f_{\text{-3 dB}}$ of unpackaged non-mesa-etched blue-emitting semipolar $(11\bar{2}2)$ LEDs. The measured $f_{\text{-3 dB}}$ of the LEDs has been found to reach 1 GHz. A back-to-back data transmission rate has been found to reach above 2.4 Gbps. These values are significantly higher than those of (0001) LEDs. This suggests that $(11\bar{2}2)$ LED is a strong candidate for VLC systems.

The LED structures were grown on high quality $(11\bar{2}2)$ GaN templates, which were prepared on patterned $(10\bar{1}2)$ *r*-plane sapphire substrates by metalorganic vapour phase epitaxy [25]. The typical threading-dislocation and basal-stacking-fault densities of these templates were estimated to be $\sim 2 \times 10^8$ cm^{-2} and $\sim 1 \times 10^3$ cm^{-1}, respectively. The LED structures consisted of 1.5-μm-thick Si-doped n-type GaN, 100-nm-thick n-$In_{0.01}Ga_{0.99}N$, a three- or five-period InGaN/GaN (2.5 nm/6.5 nm) QW active region, 120-nm-thick Mg-doped p-type GaN, and 15 nm heavily doped p-type GaN contact layer. Details of the LED growth conditions are reported elsewhere [26].

To investigate the spectral characteristics and optical output power (P_{opt}) of unpackaged $(11\bar{2}2)$ LEDs on sapphire with different p-contact geometries including 50-μm-diameter Pd contacts (non-mesa-etched μ-LEDs), 200 × 200-μm^2 and 300 × 300-μm^2 Ni/Au contacts (macro-LEDs). The contacts were evaporated by electron beam on the p-GaN layers. P_{opt} of the LEDs was collected on-wafer under direct-current (DC) conditions from the backside of the LEDs without heat sink. A calibrated Si photodetector (Thorlabs-FDS1010) was placed in close proximity to the LEDs. The electroluminescence peak emission wavelength of the LEDs varies from 430 nm to 450 nm with less than 2-nm peak shift within an injection current (I_{inject}) ranging from 0 mA to 50 mA [20, 21, 26, 27].

Fig. 1(a) shows an example of the current-voltage characteristic curve measured on a non-mesa-etched 50-μm-diameter $(11\bar{2}2)$ LED operating at ∼450 nm. (It should be noted that this measurement has been performed between two p-contacts. One of these contacts is much larger than the 50-μm-diameter one being investigated. This larger one acts as a quasi-short to the n-side.) This LED shows a typical p-n junction characteristic with a turn-on voltage of about 4.0 V and a forward voltage of 9.8 V at 50 mA. For fully processed LEDs, i.e. with optimized n-/p-contacts, which were grown under the same conditions, the turn-on voltage was estimated to be 3.5 V [26, 27].

P_{opt} of a 50-μm-diameter $(11\bar{2}2)$ LED measured on-wafer between two p-contacts in DC mode is plotted as a function of $I(J)_{inject}$ shown in Fig. 1(b). The photograph in the inset of Fig. 1(a) displays bright blue-emission from this LED taken when $I_{inject} = 3$ mA is being injected to the device. When J_{inject} exceeded 2500 A/cm^2 ($I_{inject} = 50$ mA), this LED was failed which can be attributed to device self-heating and current crowding [28]. At $J_{inject} = 1020$ A/cm^2 ($I_{inject} = 20$ mA), P_{opt} is estimated to be about 0.81 mW, corresponding to an optical power density (P_D) of 415 mW/mm^2. It should be noted that this power was measured only from the substrate direction without an integrating sphere. There is a plenty of uncollected light in the forward and side directions (see the inset of Fig. 1(a)), and multiple amounts of this power can be collected by structuring and packaging the chips [29].

The corresponding external quantum efficiency (EQE) of the 50-μm-diameter $(11\bar{2}2)$ LED increases up to $J_{inject} \approx 510$ A/cm^2 with a maximum value of ∼1.4%, and then slowly decreases to a value of ∼1.1% at $J_{inject} = 2500$ A/cm^2 (Fig. 1(b)). Though the efficiency droop in InGaN LEDs can be explained by different mechanisms such as Auger recombination, carrier overflow, and density-activated defects [13, 14], the droop of this $(11\bar{2}2)$ LED is attributed mainly to heat generation and current crowding [28, 30], as the measurements were performed on-wafer without heat sink. This result indicates that the efficiency droop in this $(11\bar{2}2)$ LED is small, consistent with previous findings reported for $(10\bar{1}1)$ LEDs operating at ∼438 nm [18] and a $(20\bar{2}\bar{1})$ LED operating at ∼447 nm [19]. This low droop in semipolar LEDs can prevent problems for data transmission VLC systems, e.g. a reduction in transmitted signal error that has been found to be significant in systems based (0001) LEDs [15].

The small-signal frequency response of the $(11\bar{2}2)$ LEDs was measured on-wafer from the backside of the LEDs using a high-performance microwave probe (DC to 3.5 GHz) without heat sink. A sinusoidal signal with low-RF power from an Agilent 8753ES vector network analyser (VNA) was applied on top of a DC bias using a bias tee (Mini-Circuits ZFBT-6GW-FT). Keithley 2400 source meters were used as the DC power suppliers for the LEDs and photoreceiver. The light output from the LEDs was collected with two 2-cm-diameter lenses with a corresponding numerical aperture of ∼0.5, i.e. similar to that of a plastic optical fiber. SubMiniature-version-A (SMA) coaxial cables (DC to 18 GHz) with 50 Ω impedance were used as transmission lines for RF signals. A high bandwidth silicon p-i-n photodiode ($f_{-3\,dB}$ ranging from 10 kHz to 1.4 GHz) with integrated transimpedance amplifier (TIA) photoreceiver (HSA-X-S-1G4-SI) was used. The frequency response curve was recorded by the VNA at different I_{inject}. A schematic of the bandwidth measurement setup is shown in Fig. 2(a).

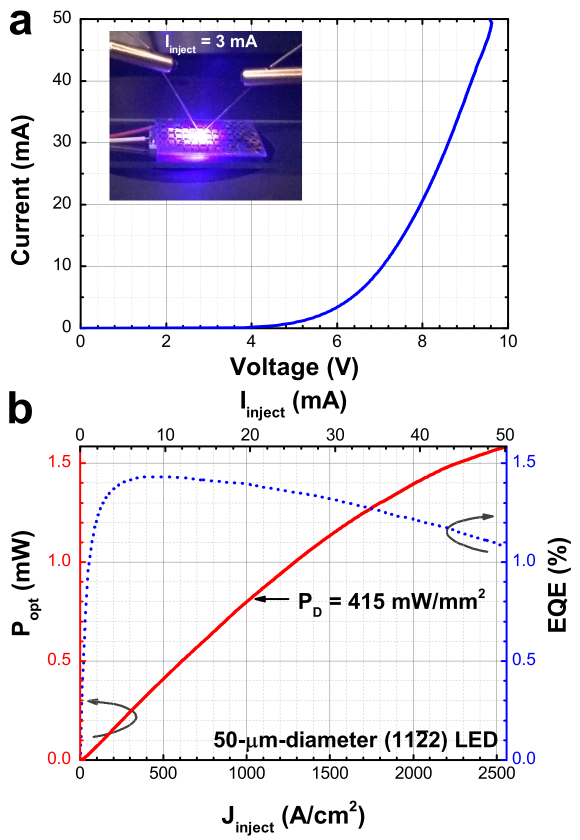

Fig. 1. (a) Current-voltage characteristic curve measured on a non-mesa-etched 50-μm-diameter $(11\bar{2}2)$ LED. The inset shows a photograph of this LED displaying bright blue emission at $I_{inject} = 3$ mA. (b) P_{opt} and corresponding EQE of this LED measured on-wafer (in the sapphire substrate direction) plotted as a function of $I(J)_{inject}$.

Fig. 2(b) shows examples of the frequency response curves of a 50-μm-diameter LED, 200 × 200-μm^2 and 300 × 300-μm^2 $(11\bar{2}2)$ LEDs measured at different J_{inject} ($I_{inject} = 4$ mA). The measured $f_{-3\,dB}$ value of these LEDs increases from 42 MHz to 1030 MHz with increasing J_{inject} from 4 A/cm^2 to 204 A/cm^2 (see also Fig. 3). This can be explained by the increased probability of bimolecular radiative recombination (reduced τ_R), which is proportional to J_{inject} injecting into the QW active volume [31]. These $f_{-3\,dB}$ values are higher than those of conventional (0001) LEDs [2, 4, 21]. This can be attributed to a shorter τ_R due to the reduced polarization-related electric fields in the $(11\bar{2}2)$ QW structures [3].

Small frequency oscillations and frequency bumps at 40 - 50 MHz are observed in the frequency response curves of the studied $(11\bar{2}2)$ LEDs (Fig. 2(b)). The oscillations are due to RF signal reflections. For LDs, such bumps have been attributed to the relaxation resonance frequency [24]. For LEDs, though frequency bumps have

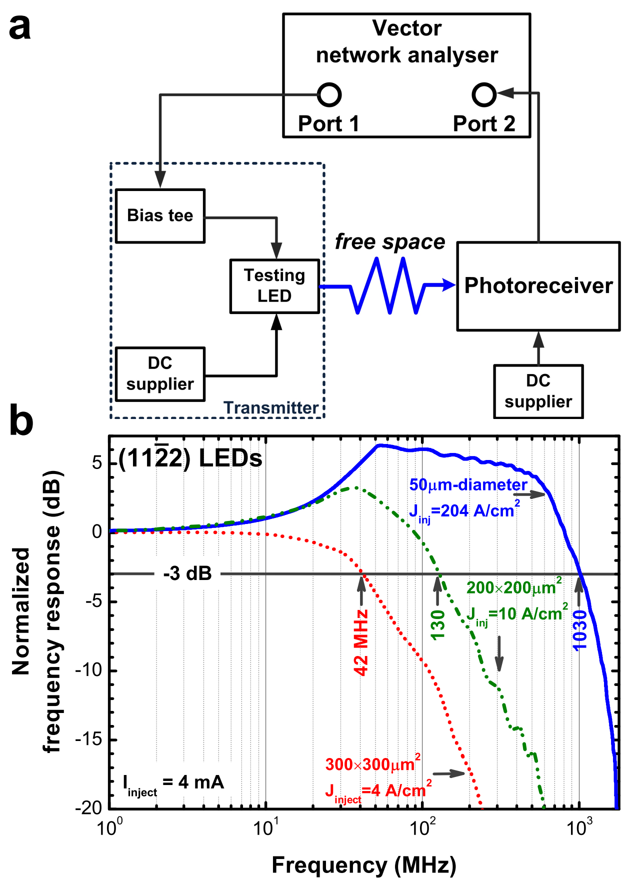

Fig. 2. (a) A schematic of the electrical-to-optical bandwidth measurement setup. (b) Normalized frequency response curves of non-mesa-etched 50-μm-diameter, 200 × 200-μm^2, and 300 × 300-μm^2 (11$\bar{2}$2) LEDs measured at different J_{inject} (I_{inject} = 4 mA).

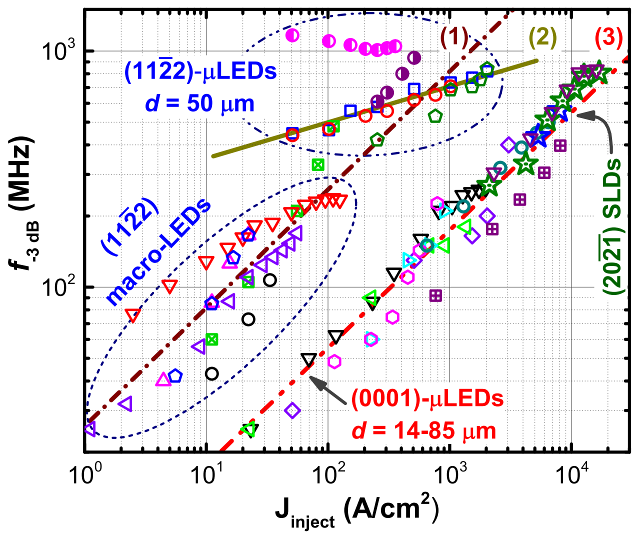

Fig. 3. The measured $f_{-3\,dB}$ values of non-mesa-etched (11$\bar{2}$2) LEDs studied here (Upper oval: five different 50-μm-diameter LEDs (◐, ◑, □, ⬠, ○); Lower oval: (▽) 200 × 200-μm^2 and (◁) 300 × 300-μm^2 macro-LEDs) are plotted as a function of J_{inject} in log-log scale. Data points previously reported for mesa-etched (14 - 85)-μm-diameter (0001) LEDs (▽ [6]; ◇, ◁, ▷ [8]; ○ [9]; ⬡ [10]; ▽, ⊞ [11]), 300 × 300-μm^2 (11$\bar{2}$2) macro-LEDs (○,⊠ [20]; △ [21] in the lower oval), a 4 × 590-μm^2 (20$\bar{2}\bar{1}$) SLD (★) [22], and a 7.5 × 1000-μm^2 (20$\bar{2}\bar{1}$) SLD (☆) [23] are also plotted for comparison. The lines (1)-(3) represent the fitting of experimental data.

been also observed for (0001) LEDs [8, 10, 32], the reason for them is still unclear and needs to be further investigated.

Fig. 3 shows $f_{-3\,dB}$ values of different non-mesa-etched 50-μm-diameter (11$\bar{2}$2) LEDs and macro-LEDs studied here plotted as a function of J_{inject}. For comparison, $f_{-3\,dB}$ values previously reported for mesa-etched (0001) μ-LEDs [6, 8–11], (11$\bar{2}$2) macro-LEDs [20, 21], and (20$\bar{2}\bar{1}$) SLDs [22, 23] are also plotted. For the (11$\bar{2}$2) μ-LEDs studied here, the measured $f_{-3\,dB}$ value has been found to reach 1 GHz for J_{inject} range of 100 - 1000 A/cm^2. Interestingly, these $f_{-3\,dB}$ values are higher than values of 560 MHz [23] and 807 MHz [22] previously reported for (20$\bar{2}\bar{1}$) SLDs, although those SLDs were measured at much higher J_{inject} of 8 kA/cm^2 [23] and 17 kA/cm^2 [22]. For (0001) μ-LEDs, the highest $f_{-3\,dB}$ value of 833 MHz has been realized for 24-μm-diameter LEDs at J_{inject} = 16 kA/cm^2 [11].

As shown in Fig. 3, despite the scattered $f_{-3\,dB}$ data points of the (11$\bar{2}$2) macro-LEDs, $f_{-3\,dB}$ - J_{inject} has been found to follow a power law: $f_{-3\,dB} \propto J^{B}_{inject}$, with an estimated (slope) B of 0.5 (see line 1 in Fig. 3). For (0001) μ-LEDs [6, 8–11] and (20$\bar{2}\bar{1}$) SLDs [22, 23], their $f_{-3\,dB}$ - J_{inject} also follow trends with B = 0.5 but they are shifted to about one order of magnitude higher J_{inject} (see line 3 in Fig. 3). According to these trends, it is therefore possible to assume that the bimolecular recombination mechanism is dominant in these LEDs [33]. It should be noted that the data points of two 50-μm-diameter (11$\bar{2}$2) LEDs studied here follow another trend with a smaller slope B = 0.15 (see line 2 in Fig. 3). For 24-μm-diameter (0001) LEDs [11], $f_{-3\,dB}$ has been found to increase with increasing J_{inject}, and then saturate at the three highest J_{inject} values (e.g. see ▽ of Ref. [11] in Fig. 3). This saturation has been attributed to the *RC* limitations [11], which can be used to explain the trend (i.e. line 2) observed for the (11$\bar{2}$2) μ-LEDs studied here.

As shown in Fig. 3, to achieve a similar $f_{-3\,dB}$ value obtained for the (11$\bar{2}$2) LEDs, (0001) LEDs have to be driven at about one order of magnitude higher J_{inject}. This can be attributed to a shorter effective carrier lifetime (τ_R) in the (11$\bar{2}$2) LEDs, resulting in a higher $f_{-3\,dB}$. The τ_R - $f_{-3\,dB}$ can be described as: $\tau_R = \sqrt{3}\cdot(2\cdot\pi\cdot f_{-3\,dB})^{-1}$ [34]. According to the data points shown in Fig. 3, at J_{inject} = 100 A/cm^2 (1000 A/cm^2) a calculated τ_R for (0001) LEDs is ~5.0 ns (1.4 ns), about 4 times longer than that of (11$\bar{2}$2) LEDs, which is ~1.2 ns (0.35 ns). This is consistent with previous results reported for (0001) and (11$\bar{2}$2) LEDs [11, 17].

To show that the (11$\bar{2}$2) LEDs can be actually used for data transmission, their transmission data rates were also investigated. Data has been sent over several centimetres of free space with the same collecting setup. A 2^7 - 1 non-return-to-zero on–off-keying (NRZ-OOK) pseudo-random bit sequence (PRBS)-7 from a pattern signal generator (Anritsu MP1632A) has been added at each DC bias. The large signal properties/back-to-back data transmission rates (i.e. "eye diagram") were collected by a digital oscilloscope (Agilent Infiniium DSO80804A). When a 2 V peak-to-peak amplitude is applied as the large signal modulation with these LEDs being biased at different I_{inject}. The transmitted data rate of non-mesa-etched 50-μm-diameter LEDs (tested on 5 different devices) has been found to exceed 2.4 Gbps (close to the limit of the photoreceiver) at $I_{inject} \geq$ 10 mA ($J_{inject} \geq$ 510 A/cm^2). Fig. 4 shows examples of eye diagrams at 2.0 Gbps and 2.4 Gbps measured on a non-mesa-etched 50-μm-diameter LED, while this LED was being biased at 10 mA. For the 300 × 300-μm^2 LEDs, the rate has been found to exceed 600 Mbps

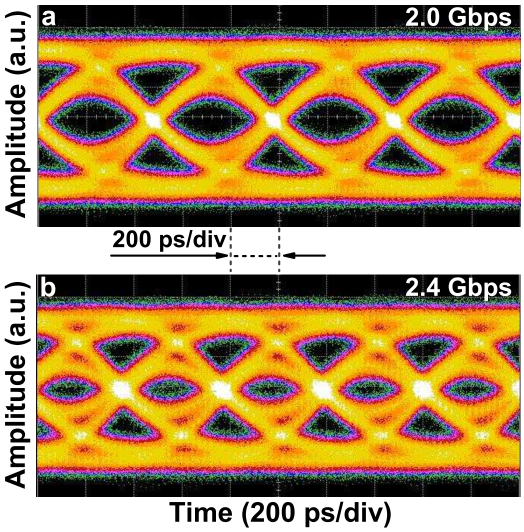

Fig. 4. Eye diagrams at (a) 2.0 Gbps and (b) 2.4 Gbps of a non-mesa-etched 50-μm-diameter $(11\bar{2}2)$ LED measured at $I_{inject} = 10$ mA.

measured at $I_{inject} = 50$ mA ($J_{inject} = 55$ A/cm^2). These high switching speeds and high data rates of $(11\bar{2}2)$ LEDs indicate that they can also be used as photodetectors in the visible range to supplement to the existing Si-based photodetectors.

Higher data rates can be achieved by using higher-level encoding methods [2, 6–8, 11, 24]. Pulse-amplitude modulation (PAM) and orthogonal frequency division multiplexing (OFDM) modulation schemes have been used with (0001) μ-LEDs ($f_{-3\,dB} = 833$ MHz) to demonstrate data transmission over free space at rates of 3.4 Gbps and 5 Gbps, respectively [11]. Thus, it can be concluded that $(11\bar{2}2)$ LEDs can be used to provide even faster data communication rates.

In conclusion, the electrical-to-optical modulation bandwidths of blue semipolar $(11\bar{2}2)$ InGaN LEDs have been investigated. The measured $f_{-3\,dB}$ of the LEDs was up to 1 GHz. A back-to-back data transmission rate has been found to reach above 2.4 Gbps. This indicates that by the use of $(11\bar{2}2)$ LEDs will enable Gbps data transmission rate for VLC systems.

Funding. This work was financially supported by the EU-FP7 ALIGHT project under agreement no. FP7-280587 and by Science Foundation Ireland through the IPIC programme (12/RC/2276).

REFERENCES

1. C. J. Humphreys, MRS Bulletin **33**, 459 (2008).
2. H. Elgala, G. Parry, and H. Haas, IEEE Commun. Mag. **49**, 56 (2011).
3. F. Bernardini, V. Fiorentini, and D. Vanderbilt, Phys. Rev. B **56**, R10024 (1997).
4. M. Akhter, P. Maaskant, B. Roycroft, B. Corbett, P. de Mierry, B. Beaumont, and K. Panzer, Electron. Lett. **38**, 1457 (2002).
5. H. L. Minh, D. O'Brien, G. Faulkner, L. Zeng, K. Lee, D. Jung, and E. T. Won, IEEE Photon. Technol. Lett. **20**, 1243 (2008).
6. J. Mckendry, R. P. Green, A. E. Kelly, Z. Gong, B. Guilhabert, D. Massoubre, E. Gu, and M. D. Dawson, IEEE Photon. Tech. Lett. **22**, 1346 (2010).
7. J. Mckendry, D. Massoubre, S. Zhang, B. R. Rae, R. P. Green, E. Gu, R. K. Henderson, A. E. Kelly, and M. D. Dawson, J. Lightware Technol. **31**, 1211 (2012).
8. J.-M. Wun, C.-W. Lin, W. Chen, J.-K. Sheu, C.-L. Lin, Y.-L. Li, J. E. Bowers, J.-W. Shi, J. Vinogradov, R. Kruglov, and O. Ziemann, IEEE Photon. J. **4**, 1520 (2012).
9. P. P. Maaskant, H. Shams, M. Akhter, W. Henry, M. J. Kappers, D. Zhu, C. J. Humphreys, and B. Corbett, Appl. Phys. Express **6**, 022102 (2013).
10. C. L. Liao, C. L. Ho, Y. F. Chang, C.-H. Wu, and M. C. Wu, IEEE Electron Dev. Lett. **35**, 563 (2014).
11. R. X. G. Ferreira, E. Xie, J. J. D. McKendry, S. Rajbhandari, H. Chun, G. Faulkner, S. Watson, A. E. Kelly, E. Gu, R. V. Penty, I. H. White, D. C. O'Brien, and M. D. Dawson, IEEE Photon. Tech. Lett. **28**, 2023 (2016).
12. C. Yang, A. A. Bettiol, Y. Shi, M. Bosman, H. R. Tan, W. P. Goh, J. H. Teng, and E. J. Teo, Adv. Optical Mater. **3**, 1703 (2015).
13. G. Verzellesi, D. Saguatti, M. Meneghini, F. Bertazzi, M. Goano, G. Meneghesso, and E. Zanoni, J. Appl. Phys. **114**, 071101 (2013).
14. P. Tian, J. J. D. McKendry, J. Herrnsdorf, S. Watson, R. Ferreira, I. M. Watson, E. Gu, A. E. Kelly, and M. D. Dawson, Appl. Phys. Lett. **105**, 171107 (2014).
15. H. Lu, C. Yan, W. Gao, T. Yu, and J. Wang, Optic. Eng. **55**, 027109 (2016).
16. M. Funato, A. Kaneta, Y. Kawakami, Y. Enya, K. Nishizuka, M. Ueno, and T. Nakamura, Appl. Phys. Express **3**, 021002 (2010).
17. Y. Ji, W. Liu, T. Erdem, R. Chen, S. T. Tan, Z.-H. Zhang, Z. Ju, X. Zhang, H. Sun, X. W. Sun, Y. Zhao, S. P. DenBaars, S. Nakamura, and H. V. Demir, Appl. Phys. Lett. **104**, 143506 (2014).
18. C.-H. Chiu, D.-W. Lin, C.-C. Lin, Z.-Y. Li, W.-T. Chang, H.-W. Hsu, H.-C. Kuo, T.-C. Lu, S.-C. Wang, W.-T. Liao, T. Tanikawa, Y. Honda, M. Yamaguchi, and N. Sawaki, Appl. Phys. Express 4, 012105 (2011).
19. C.-C. Pan, S. Tanaka, F. Wu, Y. Zhao, J. S. Speck, S. Nakamura, S. P. DenBaars, and D. Feezell, Appl. Phys. Express **5**, 062103 (2012).
20. B. Corbett, Z. H. Quan, D. V. Dinh, G. Kozlowski, D. O'Mahony, M. Akhter, S. Schulz, P. P. Parbrook, P. Maaskant, M. Caliebe, M. Hocker, K. Thonke, F. Schol, M. Pristovsek, Y. Han, C. J. Humphreys, F. Brunner, M. Weyers, T. M. Meyer, and L. Lymperakis, Proc. SPIE **9768**, 97681G-1 (2016).
21. Z. Quan, D. V. Dinh, S. Presa, B. Roycroft, A. Foley, M. Akhter, D. O'Mahony, P. P. Maaskant, M. Caliebe, F. Scholz, P. J. Parbrook, and B. Corbett, IEEE Photon. J. **8**, 1 (2016).
22. C. Shen, C. Lee, T. K. Ng, S. Nakamura, J. S. Speck, S. P. Denbaars, A. Y. Alyamani, M. M. El-desouki, and B. S. Ooi, Opt. Express **24**, 20281 (2016).
23. C. Shen, T. K. Ng, J. T. Leonard, A. Pourhashemi, S. Nakamura, S. P. Denbaars, J. S. Speck, A. Y. Alyamani, M. M. El-desouki, and B. S. Ooi, Opt. Lett. **41**, 2608 (2016).
24. C. Lee, C. Zhang, D. L. Becerra, S. Lee, C. A. Forman, S. H. Oh, R. M. Farrell, J. S. Speck, S. Nakamura, J. E. Bowers, and S. P. DenBaars, Appl. Phys. Lett. **109**, 101104 (2016).
25. F. Brunner, U. Zeimer, F. Edokam, W. John, D. Prasai, O. Krüger, and M. Weyers, Phys. Status Solidi (B) **252**, 1189 (2015).
26. D. V. Dinh, M. Akhter, S. Presa, G. Kozlowski, D. O'Mahony, P. P. Maaskant, F. Brunner, M. Caliebe, M. Weyers, F. Scholz, B. Corbett, and P. J. Parbrook, Phys. Status Solidi (A) **212**, 2196 (2015).
27. D. V. Dinh, B. Corbett, P. J. Parbrook, I. L. Kowslow, M. Rychetsky, M. Guttmann, T. Wernicke, M. Kneissl, C. Mounir, U. Schwarz, J. Glaab, C. Netzel, F. Brunner, and M. Weyers, J. Appl. Phys. **120**, 135701 (2016).
28. Z. Gong, S. Jin, Y. Chen, J. McKendry, D. Massoubre, I. M. Watson, E. Gu, and M. D. Dawson, J. Appl. Phys. **107**, 013103 (2010).
29. S. Liu, and X. Luo, in "LED packaging for lighting applications: design, manufacturing, and testing," John Wiley & Son and Chemical Industry Press (2011).
30. A. Keppens, W. R. Ryckaert, G. Deconinck, and P. Hanselaer, J. Appl. Phys. **104**, 093104 (2008).
31. K. Ikeda, S. Horiuchi, T. Tanaka, and W. Susaki, IEEE Trans. Electron Dev. **24**, 1001 (1977).
32. J.-W. Shi, J.-K. Sheu, C.-H. Chen, G.-R. Lin, and W.-C. Lai, IEEE Electron Dev. Lett. **29**, 158 (2008).
33. R. Wirth, B. Mayer, S. Kugler, and K. Streubel, Proc. SPIE **6013**, 60130F-1 (2005).
34. G. P. Agrawal, "Fiber-optic communication systems," 3rd Ed., Chap. 3, p. 90-91, John Wiley & Sons (2002).

REFERENCES

1. C. J. Humphreys, "Solid-state lighting," MRS Bulletin **33**, 459 (2008).
2. H. Elgala, G. Parry, and H. Haas, "Indoor optical wireless communication: potential and state-of-the-art," IEEE Commun. Mag. **49**, 56 (2011).
3. F. Bernardini, V. Fiorentini, and D. Vanderbilt, "Spontaneous polarization and piezoelectric constants of III-V nitrides," Phys. Rev. B **56**, R10024 (1997).
4. M. Akhter, P. Maaskant, B. Roycroft, B. Corbett, P. de Mierry, B. Beaumont, and K. Panzer, "200 Mbit/s data transmission through 100 meters of plastic optical fibre with nitride LEDs," Electron. Lett. **38**, 1457 (2002).
5. H. L. Minh, D. O'Brien, G. Faulkner, L. Zeng, K. Lee, D. Jung, and E. T. Won, "High-speed visible light communications using multiple-resonant equalization," IEEE Photon. Technol. Lett. **20**, 1243 (2008).
6. J. Mckendry, R. P. Green, A. E. Kelly, Z. Gong, B. Guilhabert, D. Massoubre, E. Gu, and M. D. Dawson, "High-speed visible light communications using individual pixels in a micro light-emitting diode array," IEEE Photon. Tech. Lett. **22**, 1346 (2010).
7. J. Mckendry, D. Massoubre, S. Zhang, B. R. Rae, R. P. Green, E. Gu, R. K. Henderson, A. E. Kelly, and M. D. Dawson, "Visible-light communications using a CMOS-controlled micro-light-emitting-diode array," J. Lightware Technol. **31**, 1211 (2012).
8. J.-M. Wun, C.-W. Lin, W. Chen, J.-K. Sheu, C.-L. Lin, Y.-L. Li, J. E. Bowers, J.-W. Shi, J. Vinogradov, R. Kruglov, and O. Ziemann, "GaN-based miniaturized cyan light-emitting diodes on a patterned sapphire substrate with improved fiber coupling for very high-speed plastic optical fiber communication," IEEE Photon. J. **4**, 1520 (2012).
9. P. P. Maaskant, H. Shams, M. Akhter, W. Henry, M. J. Kappers, D. Zhu, C. J. Humphreys, and B. Corbett, "High-speed substrate-emitting micro-light-emitting diodes for applications requiring high radiance," Appl. Phys. Express **6**, 022102 (2013).
10. C. L. Liao, C. L. Ho, Y. F. Chang, C.-H. Wu, and M. C. Wu, "High-speed light-emitting diodes emitting at 500 nm with 463-MHz modulation bandwidth", IEEE Electron Dev. Lett. **35**, 563 (2014).
11. R. X. G. Ferreira, E. Xie, J. J. D. McKendry, S. Rajbhandari, H. Chun, G. Faulkner, S. Watson, A. E. Kelly, E. Gu, R. V. Penty, I. H. White, D. C. O'Brien, and M. D. Dawson, "High bandwidth GaN-based micro-LEDs for multi-Gb/s visible light communications," IEEE Photon. Tech. Lett. **28**, 2023 (2016).
12. C. Yang, A. A. Bettiol, Y. Shi, M. Bosman, H. R. Tan, W. P. Goh, J. H. Teng, and E. J. Teo, "Fast electrical modulation in a plasmonic-enhanced, V-pit-textured, light-emitting diode," Adv. Optical Mater. **3**, 1703 (2015).
13. G. Verzellesi, D. Saguatti, M. Meneghini, F. Bertazzi, M. Goano, G. Meneghesso, and E. Zanoni, "Efficiency droop in InGaN/GaN blue light-emitting diodes: physical mechanisms and remedies," J. Appl. Phys. **114**, 071101 (2013).
14. P. Tian, J. J. D. McKendry, J. Herrnsdorf, S. Watson, R. Ferreira, I. M. Watson, E. Gu, A. E. Kelly, and M. D. Dawson, "Temperature-dependent efficiency droop of blue InGaN micro-light emitting diodes," Appl. Phys. Lett. **105**, 171107 (2014).
15. H. Lu, C. Yan, W. Gao, T. Yu, and J. Wang, "Efficiency droop effects of GaN-based light-emitting diodes on the performance of code division multiple access visible-light communication system," Optic. Eng. **55**, 027109 (2016).
16. M. Funato, A. Kaneta, Y. Kawakami, Y. Enya, K. Nishizuka, M. Ueno, and T. Nakamura, "Weak carrier/exciton localization in InGaN quantum wells for green laser diodes fabricated on semi-polar $\{20\bar{2}1\}$ GaN substrates," Appl. Phys. Express **3**, 021002 (2010).
17. Y. Ji, W. Liu, T. Erdem, R. Chen, S. T. Tan, Z.-H. Zhang, Z. Ju, X. Zhang, H. Sun, X. W. Sun, Y. Zhao, S. P. DenBaars, S. Nakamura, and H. V. Demir, "Comparative study of field-dependent carrier dynamics and emission kinetics of InGaN/GaN light-emitting diodes grown on $(11\bar{2}2)$ semipolar versus (0001) polar planes," Appl. Phys. Lett. **104**, 143506 (2014).
18. C.-H. Chiu, D.-W. Lin, C.-C. Lin, Z.-Y. Li, W.-T. Chang, H.-W. Hsu, H.-C. Kuo, T.-C. Lu, S.-C. Wang, W.-T. Liao, T. Tanikawa, Y. Honda, M. Yamaguchi, and N. Sawaki, "Reduction of efficiency droop in semipolar $(1\bar{1}01)$ InGaN/GaN light emitting diodes grown on patterned silicon substrates," Appl. Phys. Express 4, 012105 (2011).
19. C.-C. Pan, S. Tanaka, F. Wu, Y. Zhao, J. S. Speck, S. Nakamura, S. P. DenBaars, and D. Feezell, "High-power, low-efficiency-droop semipolar $(20\bar{2}\bar{1})$ single-quantum-well blue light-emitting diodes," Appl. Phys. Express **5**, 062103 (2012).
20. B. Corbett, Z. H. Quan, D. V. Dinh, G. Kozlowski, D. O'Mahony, M. Akhter, S. Schulz, P. P. Parbrook, P. Maaskant, M. Caliebe, M. Hocker, K. Thonke, F. Schol, M. Pristovsek, Y. Han, C. J. Humphreys, F. Brunner, M. Weyers, T. M. Meyer, and L. Lymperakis, "Development of semipolar $(11\bar{2}2)$ LEDs on GaN templates," Proc. SPIE **9768**, 97681G-1 (2016).
21. Z. Quan, D. V. Dinh, S. Presa, B. Roycroft, A. Foley, M. Akhter, D. O'Mahony, P. P. Maaskant, M. Caliebe, F. Scholz, P. J. Parbrook, and B. Corbett, "High bandwidth freestanding semipolar $(11\bar{2}2)$ InGaN/GaN light-emitting diodes," IEEE Photon. J. **8**, 1 (2016).
22. C. Shen, C. Lee, T. K. Ng, S. Nakamura, J. S. Speck, S. P. Denbaars, A. Y. Alyamani, M. M. El-desouki, and B. S. Ooi, "High-speed 405-nm superluminescent diode (SLD) with 807-MHz modulation bandwidth," Opt. Express **24**, 20281 (2016).
23. C. Shen, T. K. Ng, J. T. Leonard, A. Pourhashemi, S. Nakamura, S. P. Denbaars, J. S. Speck, A. Y. Alyamani, M. M. El-desouki, and B. S. Ooi, "High-brightness semipolar $(20\bar{2}\bar{1})$ blue InGaN/GaN superluminescent diodes for droop-free solid-state lighting and visible-light communication", Opt. Lett. **41**, 2608 (2016).
24. C. Lee, C. Zhang, D. L. Becerra, S. Lee, C. A. Forman, S. H. Oh, R. M. Farrell, J. S. Speck, S. Nakamura, J. E. Bowers, and S. P. DenBaars, "Dynamic characteristics of 410 nm semipolar $(20\bar{2}\bar{1})$ III-nitride laser diodes with a modulation bandwidth of over 5 GHz," Appl. Phys. Lett. **109**, 101104 (2016).
25. F. Brunner, U. Zeimer, F. Edokam, W. John, D. Prasai, O. Krüger, and M. Weyers, "Semi-polar $(11\bar{2}2)$-GaN templates grown on 100 mm trench-patterned *r*-plane sapphire," Phys. Status Solidi (B) **252**, 1189 (2015).
26. D. V. Dinh, M. Akhter, S. Presa, G. Kozlowski, D. O'Mahony, P. P. Maaskant, F. Brunner, M. Caliebe, M. Weyers, F. Scholz, B. Corbett, and P. J. Parbrook, "Semipolar $(11\bar{2}2)$ InGaN light-emitting diodes grown on chemically-mechanically polished GaN templates," Phys. Status Solidi (A) **212**, 2196 (2015).
27. D. V. Dinh, B. Corbett, P. J. Parbrook, I. L. Kowslow, M. Rychetsky, M. Guttmann, T. Wernicke, M. Kneissl, C. Mounir, U. Schwarz, J. Glaab, C. Netzel, F. Brunner, and M. Weyers, "Role of substrate quality on the performance of semipolar $(11\bar{2}2)$ InGaN light-emitting diodes," J. Appl. Phys. **120**, 135701 (2016).
28. Z. Gong, S. Jin, Y. Chen, J. McKendry, D. Massoubre, I. M. Watson, E. Gu, and M. D. Dawson, "Size-dependent light output, spectral shift, and self-heating of 400 nm InGaN light-emitting diodes," J. Appl. Phys. **107**, 013103 (2010).
29. S. Liu, and X. Luo, in "LED packaging for lighting applications: design, manufacturing, and testing," John Wiley & Son and Chemical Industry Press (2011).
30. A. Keppens, W. R. Ryckaert, G. Deconinck, and P. Hanselaer, "High power light-emitting diode junction temperature determination from current-voltage characteristics," J. Appl. Phys. **104**, 093104 (2008).
31. K. Ikeda, S. Horiuchi, T. Tanaka, and W. Susaki, "Design parameters of frequency response of GaAs-(Ga,Al)As double heterostructure LED's for optical communications," IEEE Trans. Electron Dev. **24**, 1001 (1977).
32. J.-W. Shi, J.-K. Sheu, C.-H. Chen, G.-R. Lin, and W.-C. Lai, "High-speed GaN-based green light-emitting diodes with partially n-doped active layers and current-confined apertures," IEEE Electron Dev. Lett. **29**, 158 (2008).
33. R. Wirth, B. Mayer, S. Kugler, and K. Streubel, "Fast LEDs for polymer optical fiber communication at 650 nm," Proc. SPIE **6013**, 60130F-1 (2005).
34. G. P. Agrawal, "Fiber-optic communication systems," 3rd Ed., Chap. 3, p. 90-91, John Wiley & Sons (2002).